Analysis and Optimization of the Quadratic Damping Values of Hydraulic Dampers Added in Vibratory Roller's Cab Isolations

Tao Li

School of Mechanical and Electrical Engineering, Hubei Polytechnic University, Huangshi 435003, China.
Hubei Key Laboratory of Intelligent Convey Technology and Device, Hubei Polytechnic University, Huangshi 435000, China. E-mail: litao.hpu@gmail.com

(Received 3 September 2024; accepted 23 November 2024

The comfort efficiency of the vibratory roller cab using rubber isolations is very low under different excitation frequencies. Therefore, based on the isolation efficiency of the hydraulic isolation with its quadratic damping value, the hydraulic dampers are designed and added to the cab's rubber isolations to ameliorate the cab's ride comfort and shaking. Based on the dynamic model of the vibratory roller cab equipped with rubber isolations, the influence of the damping values of the rubber isolations in the frequency domain is analyzed. Based on these analysis results, the quadratic damping values of hydraulic dampers are calculated and optimized via optimizing the geometric dimensions of hydraulic dampers and the dynamic model of the vibratory roller cab. The efficiency of the hydraulic dampers designed and optimized are then verified experimentally. The results show that with the cab's rubber isolations use, to ensure the vibratory roller's ride comfort, the front and rear damping values of the cab's rubber isolations need to be designed in the range of $21.8 \leq c_{r1} \leq 43.6$ and $2.9 \leq c_{r2} < 5.8$ kNsm^{-1}. With the cab's rubber isolations added by the optimal hydraulic dampers of $c_{h1} = 11.06$ and $c_{h2} \leq 4.05$ kNs^{2}m^{-2}, the maximum values of the power-spectral-density of the cab's vertical and pitching accelerations are strongly reduced by 94.3% and 77.0% in comparison with cab's rubber isolations. Besides, the root-mean-square values of the cab's vertical and pitching vibrations with the optimal hydraulic dampers are also greatly decreased by 75.5% and 75.2% compared to rubber isolations. Therefore, applying the designed and optimized hydraulic dampers into the cab's rubber isolations to control the vibratory roller cab's ride comfort and shaking under the different excitation frequencies is necessary.

1. INTRODUCTION

With the vibratory rollers moving and working on deformable grounds, their speed was quite low. Thus, the vibrations from deformable grounds in the low-frequency domain greatly influenced the cab's noise and ride quality.[1–3] In the isolation system of the vibratory roller cab, the rubber materials were mainly used to design the cab's rubber isolations for reducing the cab's vibration in the low-frequency domain and the cab's noise in the high-frequency domain.[4–6] The advantages of the cab's rubber isolations using rubber materials were low cost, simple structure, and easy fabrication. However, the disadvantage of these rubber isolations was that the ability to isolate vibrations of the cab in the low-frequency domain was poor due to the damping characteristics of the rubber materials being very low. Therefore, the health and comfort of the driver were difficult to ensure in the working process of vibratory rollers.

To ameliorate the ride comfort of the vibratory roller cab in the low-frequency domain, based on the isolation efficiency of the seat suspension system using the negative stiffness structure,[7,8] the isolation system of the vibratory roller seat was added by the negative stiffness structure to enhance the seat's vertical comfort.[9,10] Besides, the cab's isolation system using the rubber isolations was studied to decrease the cab's vertical vibration and shaking by increasing the damping values of rubber materials. Based on the design of the engine's rubber mounts, to increase the isolating efficiency of the engine's rubber mounts, the hydraulic mounts using hydraulic dampers were added into the engine's rubber mounts to isolate the engine's vibration in the low-frequency domain.[11,12] The results showed that the isolation ability of hydraulic isolations was better than rubber isolations. To further ameliorate the efficiency of the engine's hydraulic isolations, based on the method of controlling the damping properties of the liquid by using the MRF (magnetorheological-fluid),[13] Engine hydraulic isolations were studied and controlled. The control result of the engine's hydraulic isolations was also better than without control.[14–16] Based on these study results of the engine's hydraulic isolations, the hydraulic isolations were also applied to the vibratory roller cab's isolations to control the cab's vertical vibration and shaking.[10,17,18] The hydraulic damper of the hydraulic isolation added into the vibratory roller cab's isolations was designed by a damping plate in the chamber of the hydraulic damper. The damping plate was connected to the cab floor while the chamber of the hydraulic damper was connected to the vibratory roller frame. The oil was filled in the chamber to increase the damping force via the eight orifices designed on the damping plate and the annular gap between the damping plate and chamber when the damping plate was

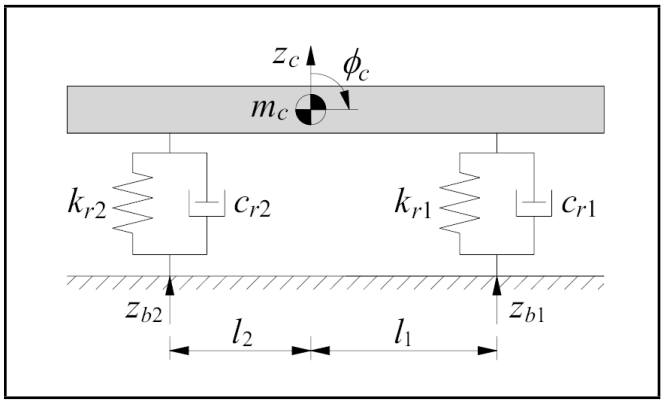

Figure 1. Isolation model of vibratory roller's cab using rubber mounts.

moving in the chamber.[19,20] To further ameliorate the quality of the vibratory roller cab using hydraulic isolations, the damping values in hydraulic isolations were controlled.[21,22] The vibratory roller's cab ride quality was better improved.

In the above studies, the front-end and rear-end hydraulic isolations applied to the vibratory roller cab's isolations were designed by the front-end and rear-end damping values with their constant damping values of $C_h = [c_{h1}, c_{h2}]$. The constant damping values were then analyzed and controlled to enhance the isolation efficiency of the hydraulic isolations. However, C_h depends greatly on the geometric dimensions of the orifice's diameter, plate's diameter, chamber's diameter, and the annular gap between the damping plate and chamber. To calculate these numerical values of C_h, all geometric dimensions of the hydraulic dampers as well as design damping parameters of the hydraulic isolations need to be analyzed in detail based on the dynamic model of the vibratory roller cab. However, these problems are ignored in all existing research.

To supplement these deficiencies, based on the dynamic model of the vibratory roller cab equipped with the rubber isolations, the influence of the damping values of the rubber isolations in the frequency domain is analyzed. Based on the analysis results, a hydraulic damper is designed and added to the cab's rubber isolations. The damping values of these designed hydraulic dampers are then calculated and optimized based on the optimization of the geometric dimensions of hydraulic dampers and dynamic model of the vibratory roller cab. The aim of this study is the design and optimization of the cab's hydraulic isolations to control the vibratory roller cab's ride comfort and shaking.

2. MODEL AND CALCULATING APPROACH

2.1. Model of Cab with Rubber Isolations

In the isolation systems of the vibratory roller cab using the rubber isolations, the physical parameters of the front-end rubber isolations are larger than the physical parameters of the rear-end rubber isolations to reduce the pitching cab vibration. However, the physical parameters between the left and right rubber isolations are the same.[21,23] Thus, to study the cab's vibration, a half model of the vibratory roller's cab using the front and rear rubber isolations is established in Fig. 1a. Where z_c, ϕ_c, and m_c are the vertical displacement, pitching angle, and mass of the cab. l_1 and l_2 are the distance between the front/rear isolations and the center of gravity of the cab. z_{b1} and z_{b2} are the front and rear vibration excitations of the cab from the vibratory roller's body. c_{r1} and k_{r1} and c_{r2} and k_{r2} are the damping and stiffness values of the cab's front and rear rubber isolations.

The vibration equations of the cab in Fig. 1b is written in the time domain as follows:[21]

$$\begin{cases} m_c\ddot{z}_c = c_{r1}\dot{Z}_1 + k_{r1}Z_1 + c_{r2}\dot{Z}_2 + k_{r2}Z_2 \\ I_c\ddot{\phi}_c = (c_{r2}\dot{Z}_2 + k_{r2}Z_2)l_2 - (c_{r1}\dot{Z}_1 + k_{r1}Z_1)l_1 \end{cases}; \quad (1)$$

where $Z_1 = z_{b1} - z_c + l_1\phi_c$ and $Z_2 = z_{b2} - z_c - l_2\phi_c$.

To evaluate the cab's vibration characteristic in the frequency domain, based on the Laplace transfer function, the transfer functions in the cab's vertical and pitching vibrations in the frequency domain calculated from Eq. (1) could be expressed by:[24]

$$\begin{cases} a_{11}Z_{c(i\omega)} + a_{12}\Phi_{c(i\omega)} = b_{11}Z_{b1(i\omega)} + b_{12}Z_{b2(i\omega)} \\ a_{21}Z_{c(i\omega)} + a_{22}\Phi_{c(i\omega)} = b_{21}Z_{b1(i\omega)} + b_{22}Z_{b2(i\omega)} \end{cases}; \quad (2)$$

where $\begin{cases} a_{11} = -m_c\omega^2 + (c_{r1} + c_{r2})i\omega + (k_{r1} + k_{r2}) \\ a_{12} = (c_{r2}l_2 - c_{r1}l_1)i\omega + (k_{r2}l_2 - k_{r1}l_1) \\ b_{11} = c_{r1}i\omega + k_{r1}, \text{ and } b_{12} = c_{r2}i\omega + k_{r2} \end{cases}$ and

$\begin{cases} a_{21} = (c_{r2}l_2 - c_{r1}l_1)i\omega + (k_{r2}l_2 - k_{r1}l_1) \\ a_{22} = -I_c\omega^2 + (c_{r1}l_1^2 + c_{r2}l_2^2)i\omega + (k_{r1}l_1^2 + k_{r2}l_2^2) \\ a_{21} = -(c_{r1}i\omega + k_{r1})l_1, \text{ and } a_{22} = (c_{r2}i\omega + k_{r2})l_2 \end{cases}$.

$Z_{c(i\omega)}, \Phi_{c(i\omega)}, Z_{b1(i\omega)}$ and $Z_{b2(i\omega)}$ are the vibrations and excitations of the cab in the frequency domain.

By dividing Eq. (2) by the front excitation of $Z_{b1(j\omega)}$, Eq. (2) is described by the following matrix:

$$\begin{bmatrix} a_{11} & a_{12} \\ a_{21} & a_{22} \end{bmatrix} \begin{Bmatrix} H_{z(i\omega)} \\ H_{\phi(i\omega)} \end{Bmatrix} = \begin{bmatrix} b_{11} & b_{12} \\ b_{21} & b_{22} \end{bmatrix} \begin{Bmatrix} 1 \\ Z_{b2(i\omega)}/Z_{b1(i\omega)} \end{Bmatrix}; \quad (3)$$

herein $H_{z(i\omega)} = \frac{Z_{c(i\omega)}}{Z_{b1(i\omega)}}$ and $H_{\phi(i\omega)} = \frac{\phi_{c(i\omega)}}{Z_{b1(i\omega)}}$ are the vibration's transfer functions from the vibratory roller's body to the cab's vertical and pitching directions.

From the parameters of the vibratory roller's cab and its isolation systems designed, both the matrices of $\Omega = \begin{bmatrix} a_{11} & a_{12} \\ a_{21} & a_{22} \end{bmatrix}$ and $\Psi = \begin{bmatrix} b_{11} & b_{12} \\ b_{21} & b_{22} \end{bmatrix}$ in Eq. (3) could be calculated. Therefore, both $H_{z(i\omega)}$ and $H_{\phi(i\omega)}$ in Eq. (3) are determined by:

$$\begin{cases} H_{z(j\omega)} = \frac{\Psi}{\Omega} \begin{bmatrix} 1 & a_{12} \\ Z_{b2(i\omega)}/Z_{b1(i\omega)} & a_{22} \end{bmatrix} \\ H_{\phi(j\omega)} = \frac{\Psi}{\Omega} \begin{bmatrix} a_{11} & 1 \\ a_{21} & Z_{b2(i\omega)}/Z_{b1(i\omega)} \end{bmatrix} \end{cases}. \quad (4)$$

By transforming Eq. (4), the obtained results of $H_{z(i\omega)}$ and $H_{\phi(i\omega)}$ are the complex number form and described by:

$$\begin{cases} H_{z(j\omega)} = A_z + iB_z \\ H_{\phi(j\omega)} = A_\phi + iB_\phi \end{cases}. \quad (5)$$

From the complex number equations of $H_{z(i\omega)}$ and $H_{\phi(i\omega)}$ in Eq. (5), the relationship between the excitation frequency

Table 1. Simulation parameters of the cab and its isolations.

Parameter	Value	Parameter	Value
m_c/kg	445	k_{r1}/Nm^{-1}	9.1×10^5
c_{r1}/Nsm^{-1}	218	k_{r2}/Nm^{-1}	1.2×10^5
c_{r2}/Nsm^{-1}	29	l_1/m	0.100
I_c/kgm^2	280	l_2/m	0.524

Table 2. Results of the maximum $|\ddot{H}_{z(j\omega)}|$ and $|\ddot{H}_{\phi(j\omega)}|$.

Damping values	Max $\lvert\ddot{H}_{z(j\omega)}\rvert$	Max $\lvert\ddot{H}_{\phi(j\omega)}\rvert$
$\lambda = 0$	128.7	152.0
$\lambda = 1$	52.1	101.7
$\lambda = 50$	26.7	59.4
$\lambda = 100$	18.3	38.4
$\lambda = 200$	13.6	28.0

and acceleration response in the cab's vertical and pitching directions could be expressed by:[24]

$$\begin{cases} |\ddot{H}_{z(j\omega)}| = \omega^2\sqrt{A_z^2 + B_z^2} \\ |\ddot{H}_{\phi(j\omega)}| = \omega^2\sqrt{A_\phi^2 + B_\phi^2} \end{cases}; \tag{6}$$

herein $\omega = 2\pi f$ and f is the excitation frequency of the cab's vibration model from the vibratory roller's body.

Eq. (6) was then applied to evaluate the cab's vibration characteristics in the frequency domain.

2.2. Cab's Vibration Characteristic under the Influence of Damping Values

With the design parameters of the vibratory roller's cab using the rubber isolations provided in Table 1,[21,23] these parameters were then simulated to evaluate the cab's vibration characteristics in the frequency domain under the influence of damping values $C = \lambda \times [c_{r1}, c_{r2}]$, here $\lambda = \{0, 1, 50, 100, 200\}$. The relationship result between the excitation frequencies and acceleration responses in the cab's vertical and pitching directions are shown in Figs. 2a and 2b. Besides, the maximum values of $|\ddot{H}_{z(j\omega)}|$ and $|\ddot{H}_{\phi(j\omega)}|$ are listed in Table 2.

Figs. 2a and 2b show that with the cab's isolation system using the front and rear rubber mounts with their stiffness values of k_{r1} and k_{r2}, the two resonant frequencies of the cab's isolation system appear at $f_1 = 2.0$ and $f_2 = 7.7$ Hz. At these two resonant frequencies, the amplitude-frequency responses of the cab's vertical acceleration and pitching acceleration are strongly affected by the change in the damping value of C. With the cab's isolation system without the damping value of $C(\lambda = 0)$, the amplitude-frequency responses of $|\ddot{H}_{z(j\omega)}|$ and $|\ddot{H}_{\phi(j\omega)}|$ are very high. However, with the small damping values of c_{r1} and c_{r2} added in the cab's isolation system ($\lambda = 1$), the maximum values of $|\ddot{H}_{z(j\omega)}|$ and $|\ddot{H}_{\phi(j\omega)}|$ in Table 2 are strongly reduced by 59.5% and 33.1% in comparison without C. This implies that the damping values must be added to the cab's isolation system to improve ride comfort. However, with the damping values of the cab's rubber mounts designed by $c_{r1} = 218$ and $c_{r1} = 29$ Nsm^{-1},[21,23,25] the maximum values of $|\ddot{H}_{z(j\omega)}|$ and $|\ddot{H}_{\phi(j\omega)}|$ are still very high. This means that the cab's ride comfort is very poor.

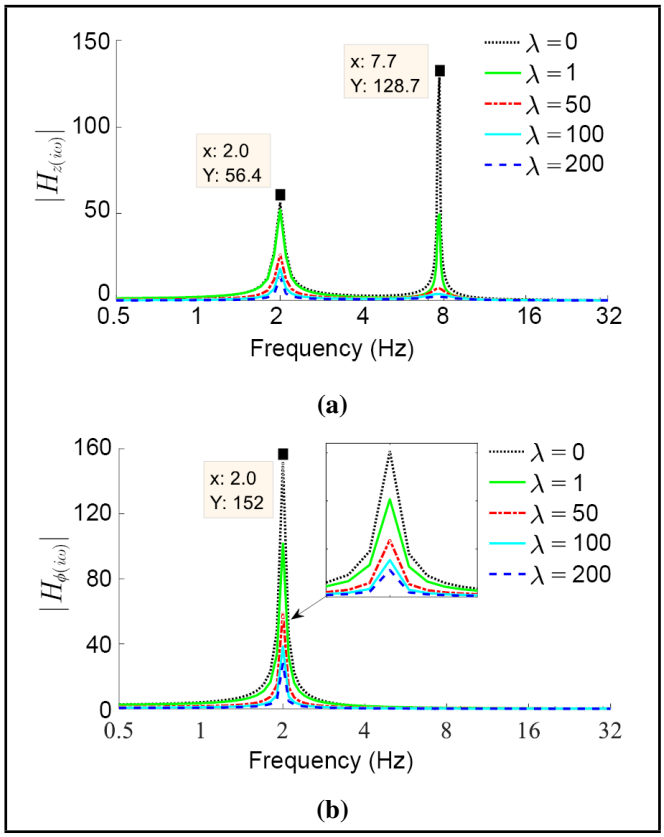

Figure 2. (a) Characteristic of cab's vertical acceleration. (b) Characteristic of cab's pitching acceleration.

Thus, the damping value of C needed to be increased. With the increase of the C at $\lambda = \{50, 100, 200\}$, the results in the same Figs. 2a and 2b indicate that $|\ddot{H}_{z(j\omega)}|$ and $|\ddot{H}_{\phi(j\omega)}|$ are still greatly reduced. Especially, λ increases from 50–200, the maximum values of $|\ddot{H}_{z(j\omega)}|$ and $|\ddot{H}_{\phi(j\omega)}|$ are greatly reduced from 59.5%– 89.4% and 33.1%–81.6% in comparison without $C(\lambda = 0)$. However, when $\lambda > 200$, the maximum values of $|\ddot{H}_{z(j\omega)}|$ and $|\ddot{H}_{\phi(j\omega)}|$ are insignificantly reduced in comparison with their values at $\lambda = 200$. Accordingly, to ensure the ride comfort of the vibratory roller, the damping values of the cab's rubber isolations should be designed by $\lambda \geq 50 (c_{r1} \geq 10.9 \times 10^3 \text{and} c_{r2} \geq 1.45 \times 10^3$ Nsm^{-1}). However, both c_{r1} and c_{r2} are difficult to achieve in these ranges if the cab's isolations are designed and used by rubber materials with $c_{r1} = 218$ and $c_{r2} = 29$ in Table 1.

To solve this problem, the cab's rubber isolations added by the hydraulic dampers to increase the damping values will be designed and calculated in the next section.

2.3. Design of Cab's Hydraulic Isolation

Based on the structure of the cab's rubber systems used in the vibratory roller cab in Fig. 3a,[25] a hydraulic damper was designed and added to the rubber mount to enhance its damping value. Its structure and mathematical model are plotted in Figs. 3b and 3c. Where D_1, D_2, and D_3 are the diameters of the chamber, damping plate, and orifice. k_r and c_r are the stiffness and damping values of the rubber material in the rubber mount. H is the annular gap.

To calculate the dynamic equation of the designed hydraulic damper (DHD), some assumptions are made as follows: (1)

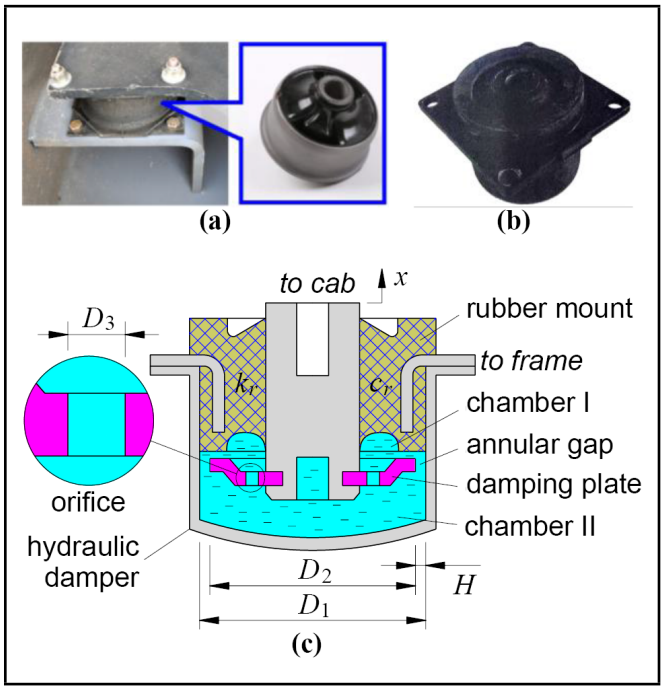

Figure 3. (a) Rubber isolation. (b) Hydraulic isolation. (c) Mathematical model of hydraulic isolation.

the inertia and friction of the oil in the chamber are very small, (2) the temperature and density of the oil are stable during the working process of DHD, (3) the damping plate mainly works in the vertical direction, and (4) the vertical deformation of DHD is x. Based on the study results presented by Jiao, Wang, Zhang, Hua[19] and Nguyen,[25] when the damping plate is moving in the chamber, the moving velocities of the oil generated at the orifice and annular gap are v_o and v_a. The pressure losses of the oil at the orifice and annular gap are expressed by:

$$\Delta p_o = \frac{\delta_o \rho}{2}|v_o|v_o \text{ and}$$
$$\Delta p_a = \frac{\delta_a \rho}{2}|v_a|v_a; \tag{7}$$

herein ρ is the oil's density, δ_o and δ_a are the loss coefficients of the oil at the orifice and annular gap.

Under the influence of the effective areas in the chamber (A_1), annular gap (A_2), and orifice (A_3) of DHD, both δ_o and δ_a in Eq. (7) are determined by:[19]

$$\delta_o = \frac{A_1 - A_3}{2A_1} = \frac{D_1^2 - jD_3^2}{2D_1^2} \text{ and } \delta_a = \frac{A_1 - A_2}{2A_1} = \frac{D_2^2}{2D_1^2}; \tag{8}$$

where $A_1 = \frac{\pi D_1^2}{4}$, $A_2 = \frac{\pi(D_1^2 - D_2^2)}{4}$, and $A_3 = \frac{j\pi D_3^2}{4}$. j is the orifice number on the plate.

The flow ratio of the oil in chamber I and chamber II through the orifice and annular gap is determined based on the continuous flow equation of the oil as follows:[25]

$$Q = A_1\dot{x} = S_3 v_o = S_2 v_a. \tag{9}$$

By substituting the values of A_1, A_2, and A_3 from Eq. (8) into Eq. (9) and transforming Eq. (9), both v_o and v_a can be determined by:

$$v_o = \frac{D_1^2}{D_1^2 - D_2^2}\dot{x} \text{ and } v_a = \frac{D_1^2}{jD_3^2}\dot{x}. \tag{10}$$

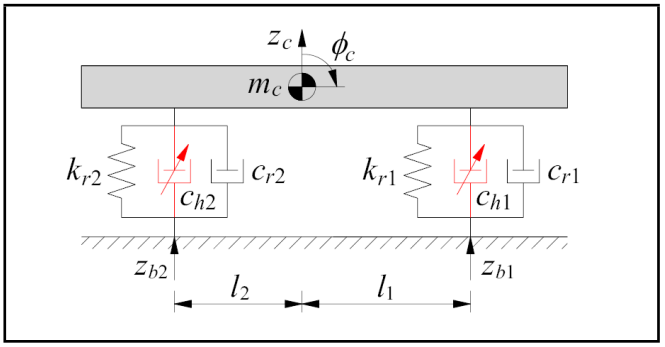

Figure 4. Isolation model of vibratory roller's cab using hydraulic isolations.

Based on the pressure losses of the oil at the orifice and annular gap determined by Δp_o and Δp_a in Eq. (7), the difference in the oil pressure in the hydraulic damper is written as follows:

$$\Delta p = \Delta p_o + \Delta p_a. \tag{11}$$

Therefore, the force response of DHD generated by the influence of the difference of the oil pressure (Δp) on the damping plate's area (A_4) is expressed by:

$$F_h = \Delta p \times A_4 = c_h|\dot{x}|\dot{x}; \tag{12}$$

where A_4 is calculated by $A_4 = \pi(D_2^2 - jD_3^2)/4$ and c_h is the quadratic damping value of DHD.

The c_h depends on the geometric dimensions of DHD and it is described as follows:

$$c_h = \frac{\psi}{16}\left[\frac{D_2^2}{(D_1^2 - D_2^2)^2} + \frac{D_1^2 - jD_3^2}{j^2 D_3^4}\right]; \tag{13}$$

where $\psi = \rho\pi(D_2^2 - jD_3^2)D_1^2$.

Based on the quadratic damping value c_h of DHD added in the cab's front and rear rubber isolations, the vibration model of the vibratory roller's cab using front and rear hydraulic isolations is established in Fig. 4.

Therefore, the vibration equations of the cab added by DHD in Fig. 4 can be rewritten by:

$$\begin{cases} m_c\ddot{z}_c = (c_{r1} + c_{h1}|\dot{x}_1|)\dot{x}_1 + k_{r1}x_1 + \\ \quad (c_{r2} + c_{h2}|\dot{x}_2|)\dot{x}_2 + k_{r2}x_2 \\ I_c\ddot{\phi}_c = [(c_{r2} + c_{h2}|\dot{x}_2|)\dot{x}_2 + k_{r2}x_2)]l_2 - \\ \quad [(c_{r1} + c_{h1}|\dot{x}_1|)\dot{x}_1 + k_{r1}x_1]l_1 \end{cases}; \tag{14}$$

where $x_1 = Z_1$ and $x_2 = Z_2$. Both Z_1 and Z_2 have been calculated in Eq. (1).

Eq. (13) is applied to analyze the characteristics of c_{h1} and c_{h2}. Then, Eq. (14) is used to optimize the efficiency of DHD in isolating the vibration of the vibratory roller cab.

3. CALCULATION RESULT AND ANALYSIS

3.1. Influence of DHD Added in Cab's Rubber Isolations

The cab's vibration was mainly generated by the random excitation from the off-road ground surface. Thus, to evaluate the influence of DHD added in the cab's rubber isolation system,

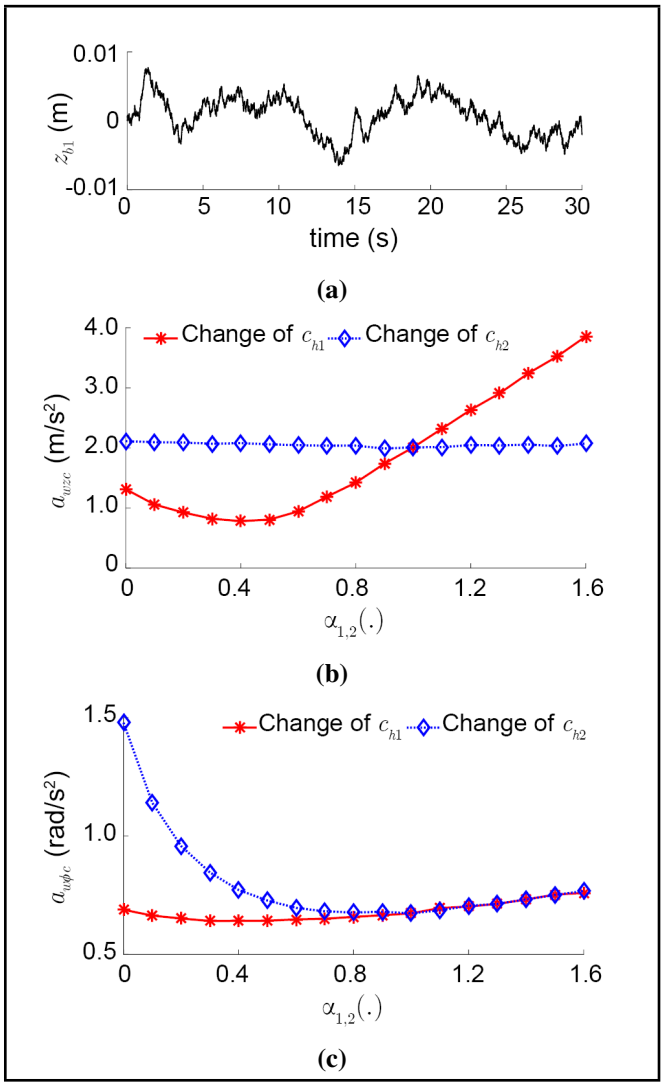

Figure 5. (a) Vibration excitation of cab floor. (b) Vertical RMS cceleration. (c) Pitching RMS acceleration of cab.

the random excitations of z_{b1} and $z_{b1} = z_{b1}\{t = (l_1 + l_2)/v\}$ computed from the random excitation of the off-road ground surface via ISO 8068 class D and vibratory roller model were applied for the simulation.[2,26] The excitation result of z_{b1} at a low speed of the vibratory roller of $v = 10$ km/h is shown in Fig. 5a.

Based on the dynamic parameters of the cab's rubber isolations in Table 1 and initial parameters of the cab's front and rear hydraulic dampers with $c_{h1} = 20 \times 10^3$ and $c_{h2} = 4.5 \times 10^3$ Ns^{2}m^{-2},[21,23] under the change of $C_h = [\alpha_1 \times c_{h1}, \alpha_2 \times c_{h2}]$ with $\alpha_{1,2}$ increasing from 0.0 to 1.6, the cab's vertical root-mean-square (RMS) acceleration (a_{wzc}) and pitching RMS acceleration $(a_{w\phi c})$ calculated by $a_{wk} = \sqrt{\int_{0.5}^{80} w_{(f)}^2 a_{k(f)} df}$ in the frequency domain[27,28] are plotted in Figs. 5b and 5c.

Reducing the a_{wzc} and $a_{w\phi c}$ of the cab also means increasing the ride comfort and the durability of the structures. Thus, a_{wzc} and $a_{w\phi c}$ are used to evaluate the influence of DHA on the cab's ride comfort.

Figs. 5b and 5c show that a_{wzc} is strongly increased while $a_{w\phi c}$ is insignificantly changed with the increase of c_{h1}. Conversely, a_{wzc} is insignificantly changed while $a_{w\phi c}$ is significantly affected by the increase of c_{h2}. This means that c_{h1} strongly affects the cab's vertical ride comfort while c_{h2} significantly affects the cab's shaking. Both a_{wzc} and $a_{w\phi c}$ attain their minimum values when c_{h1} and c_{h2} are designed within the ranges of $\alpha_1 \times c_{h1}$ with $0.3 < \alpha_1 < 0.7$ and $\alpha_2 \times c_{h2}$ with $0.7 < \alpha_2 < 1.1$. Thus, to improve both the cab's vertical vibration and shaking, the damping values of the front and rear hydraulic dampers should be designed in the ranges of $6 \times 10^3 < c_{h1} < 14 \times 10^3$ and $3.15 \times 10^3 < c_{h2} < 4.95 \times 10^3$ Ns^{2}m^{-2}.

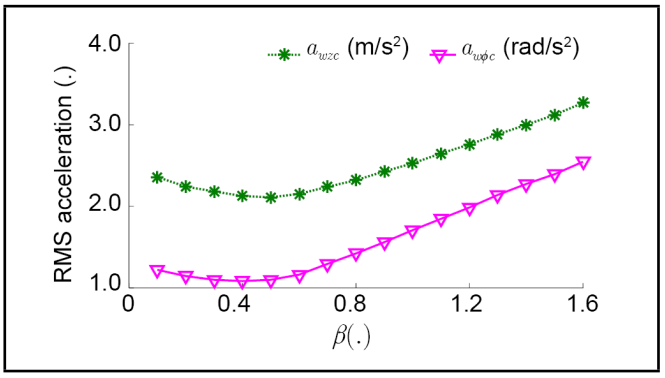

Figure 6. Change of the damping ratio between the cab's front and rear hydraulic dampers.

Besides, the damping ratio between the cab's front and rear vibration isolations is $\beta = c_{h1}/c_{h2} = 4.44$.[21,23] However, the change of this damping ratio can also affect both the cab's vertical vibration and shaking. Thus, a change range of β from 0.5 to 8.0 is also simulated to evaluate the influence of β. The simulated result is presented in Fig. 6.

The result shows that both a_{wzc} and $a_{w\phi c}$ attain their minimum values when the damping ratio is changed in a range of $1.0 < \beta < 3.0$. When the β is increased from 3.0 to 8.0, both a_{wzc} and $a_{w\phi c}$ are strongly increased. Thus, the cab's ride comfort is very poor. This is the reason why in the design of the cab isolation system of off-road vibratory rollers, the damping values of the front-end isolations are usually higher than those of the rear-end isolations.[21,23] However, in the existing studies of the vibratory roller cab using hydraulic isolations, these damping values are not optimized. Thus, optimizing c_{h1} and c_{h2} to enhance the cab's vertical vibration and shaking is necessary.

Based on hydraulic isolation designed in Fig. 3 as well as its quadratic damping value calculated in Eq. (13), we can see that the damping values of c_{h1} and c_{h2} depend on the geometric dimensions of D_1, D_2, and D_3. This means that to optimize c_{h1} and c_{h2}, the influence of D_1, D_2, and D_3 on the damping characteristic of DHD needs to be evaluated, and these geometric dimensions need to be optimized.

3.2. Influence of Geometric Dimensions of DHD

Influence of the orifice's diameter and number: Based on the basic geometric dimensions of a hydraulic damper listed in Table 3,[19] to evaluate the influence of the orifice diameter (D_3) and orifice number (j) on the damping characteristics of $C_h = [c_{h1}, c_{h2}]$, both D_3 and j changed in the ranges of

Table 3. The geometric dimensions of the hydraulic damper.

Parameter	Value	Parameter	Value
D_1/mm	124	H/mm	1.0
D_2/mm	122	ρ/kg m^{-3}	850
D_3/mm	10	j	8.0

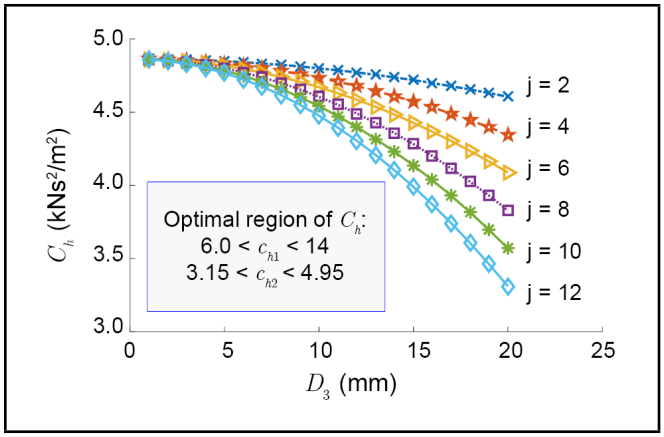

Figure 7. Influence of D_3 and j on C_h.

$1.0 < D_3 < 20$ and $2 < j < 12$ are simulated. Their influence results have been presented in Fig. 7.

Fig. 7 shows that both D_3 and j significantly affect C_h. Whith the increase of D_3 and j , the flow of oil moving through the orifices increases, thus, the fluid resistance in the orifices decreases and the damping value of C_h is reduced. Fig. 7 also shows that under the change of D_3 and j, the maximum value of the hydraulic damper is achieved by 4.86 Ns^{2}m^{-2} at $D_3 = 1.0$ and $j = 2$. However, this value only satisfies the design condition of the rear hydraulic damper with $3.15 \times 10^3 < c_{h2} < 4.95 \times 10^3$ Ns^{2}m^{-2}. Based on the design condition of the front hydraulic damper with $6 \times 10^3 < c_{h1} < 14 \times 10^3$ Ns^{2}m^{-2}, the c_{h1} is not achieved under any changes in D_3 and j. Therefore, to simplify the design of the front and rear hydraulic dampers, the geometric dimensions of $D_3 = 10$ and $j = 8$ are applied for both the front and rear hydraulic dampers.

Influence of the chamber diameter and annular gap: To assess the influence of the chamber diameter D_1 and annular gap ($H = 0.5(D_1 - D_2)$) on $C_h = [c_{h1}, c_{h2}]$, based on basic geometric dimensions of D_1 and D_2 provided in Table 3, both the changes of D_1 and H from $76 < D_1 < 196$ and $0.1 < H < 1.5$ are simulated. The simulation result is shown in Fig. 8.

Fig. 8 indicates that both D_1 and H strongly affect C_h. When D_1 is increased, the damping plate area is also increased, thus, the damping value of C_h is increased and vice versa. Conversely, when H is increased, the flow of oil moving through the annular gap is also increased. Therefore, the damping value of C_h is decreased. Based on the simulation result in Fig. 8, we can see that to satisfy the design conditions of the front and rear hydraulic dampers, the range of $124 \leq D_1 < 196$ and $0.1 < H < 1.2$ could be designed for the front hydraulic damper and the range of $100 \leq D_1 < 172$ and $0.1 < H < 1.3$ could be designed for the rear hydraulic damper. However, to simplify the manufacturing process of

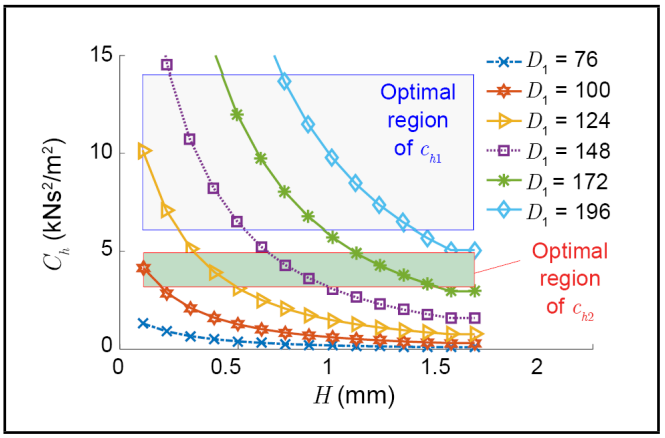

Figure 8. Influence of D_1 and H on C_h.

the front and rear hydraulic dampers, their D_1 dimensions should be uniform. Therefore, the geometric dimensions of $124 \leq D_1 \leq 148$ could be designed for both the front and rear hydraulic dampers while the annular gap of $H = H_1$ with $0.1 < H_1 < 0.5$ should be applied for the front hydraulic damper and $H = H_2$ with $0.3 < H_2 < 0.9$ should be applied for the rear hydraulic damper.

Based on the above analysis results, to enhance the efficiency of DHD of the vibratory roller cab, the geometric dimensions of D_1 and H need to be optimized based on the boundary conditions of $\{D_1, H, \beta, c_{h1}, c_{h2}\}$.

4. OPTIMIZATION OF HYDRAULIC DAMPERS

4.1. Optimization Approach

There are many methods used to optimize parameters in mathematical models, such as the micro-genetic algorithm, PID-fuzzy control, optimal neural-fuzzy control, and genetic algorithm.[22,29,30] Among them, the genetic algorithm (GA) is known as an optimization method with a simple structure but high efficiency in finding multi-objective functions. Thus, GA is applied to optimize the geometric dimensions of D_1 and H. In this study, GA is defined as finding a vector of $a = [D_1, H_1, H_2]^T$ to obtain the minimum value of $J = [a_{wzc}, a_{w\phi c}]^T$. Thus, to perform the optimization process, the geometric dimensions in a vector of a are encoded by $D_1 = [124, 125, \ldots, D_{1j}, \ldots, 147, 148]^T$, $H_1 = [0.1, 0.11, \ldots, H_{1j}, \ldots, 0.49, 0.5]^T$, and $H_2 = [0.3, 0.31, \ldots, H_{1j}, \ldots, 0.89, 0.9]^T$. These parameters are randomly chosen to calculate $C_h = [c_{h1}, c_{h2}]$ via GA and Eq. (13).

Based on the boundary conditions of the front and rear hydraulic dampers determined by $6 \times 10^3 < c_{h1} < 14 \times 10^3$, $3.15 \times 10^3 < c_{h2} < 4.95 \times 10^3$, and $1.0 < \beta < 3.0$ in section 3.1, the values of $C_h = [c_{h1}, c_{h2}]$ that satisfy the boundary conditions will be applied to calculate the minimum value (fitness value) of $J = [a_{wzc}, a_{w\phi c}]^T$ via the vibration model of cab in Fig. 4. From the initial population, the crossover probability, and the mutation probability of GA established by 200, 0.95, and 0.05 in 10^3 generations, GA is then performed based on MATLAB software. The details of the optimization process are illustrated in Fig. 9. After the optimization process is

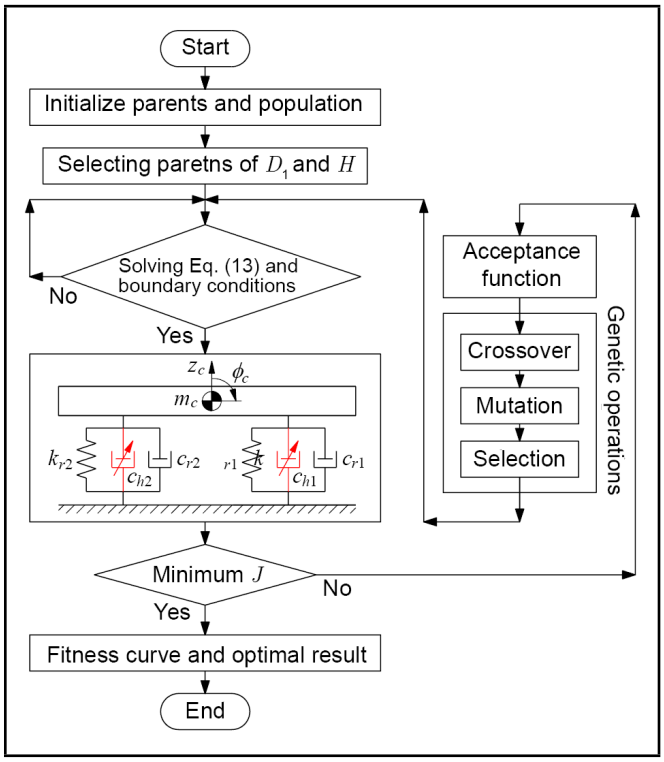

Figure 9. The GA's flow chart for the model of cab and hydraulic isolations.

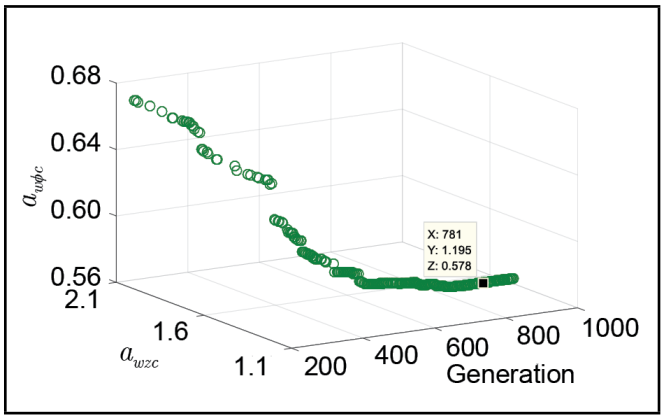

Figure 10. Fitness curve and optimal result.

finished, the smaller values of a_{wzc} and $a_{w\phi c}$ generated in the evolutionary generations are saved and plotted in Fig. 10.

The results show that the evolutionary generations are carried out from 0 to 400, both the fitness values of a_{wzc} and $a_{w\phi c}$ decrease rapidly. This is due to the high mutation probability of the optimization process, thus, the optimal values of a_{wzc} and $a_{w\phi c}$ are quickly found. When the evolutionary generations are increased from 400 to 780, the mutation probability isreduced, thus, both a_{wzc} and $a_{w\phi c}$ decrease more slowly. When the evolutionary generations are increased from 781 to the end, both a_{wzc} and $a_{w\phi c}$ remain almost unchanged. Therefore, the optimal values can be achieved from the generation of 781 to the end. By saving the optimization results in the MATLAB/Workspace, the parameters of the optimized hydraulic dampers (OHD) are provided in Table 4. From these optimal results, the efficiency of OHD will be analyzed in section 4.2.

Table 4. The optimal result of front and rear hydraulic dampers.

Parameter	DHD	OHD
β	4.44	2.73
D_1/mm	124	130.0
H_1/mm	1.0	0.22
H_2/mm	1.0	0.54
c_{h1}/kNs^{2}m^{-2}	20	11.06
c_{h2}/kNs^{2}m^{-2}	4.5	4.05

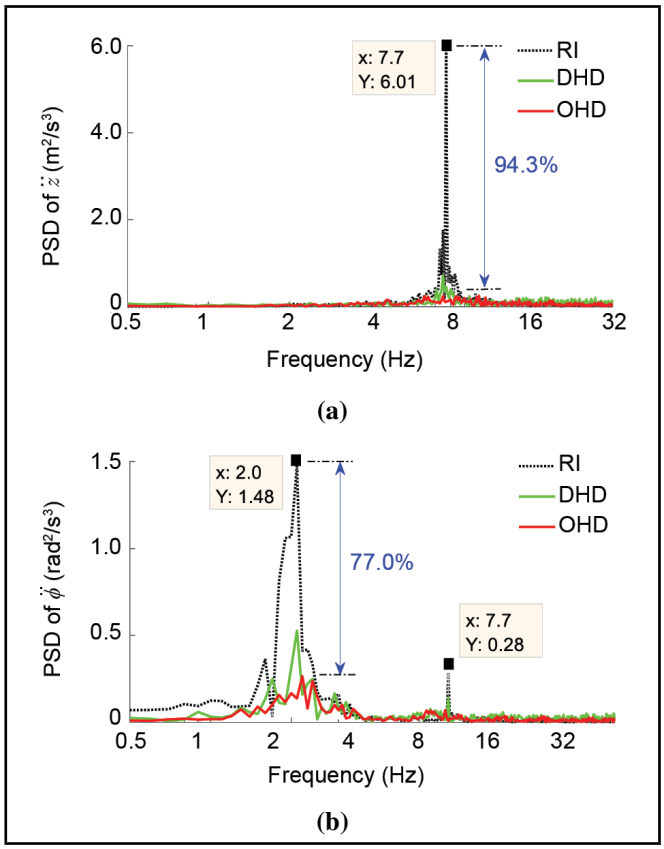

Figure 11. (a) Vertical PSD acceleration response. (b) Pitching PSD acceleration response of cab in the frequency region.

4.2. Efficiency of Optimized Hydraulic Dampers

Under the same simulation condition of the cab's vibration model in Section 3, three different cases of the cab's isolations using RI, DHD, and OHD are then simulated. Results of the power-spectral-density (PSD) of the cab's vertical and pitching acceleration responses in the frequency domain are plotted in Figs. 11a and 11b.

By adding OHD in the cab's RI, the two resonant frequencies of the cab's isolation system also appear at $f_1 = 2.0$ and $f_2 = 7.7$ Hz. It is like the simulation results in section 2.2. This is because the stiffness of the cab's isolation system does not change while the resonance frequencies of the system are not affected by the damping values. However, at these two resonant frequencies, the maximum values of the PSD of the cab's vertical and pitching accelerations with OHD are strongly reduced in comparison with both RI and DHD. Especially, these PSD values with OHD are smaller than those of RI by 94.3%

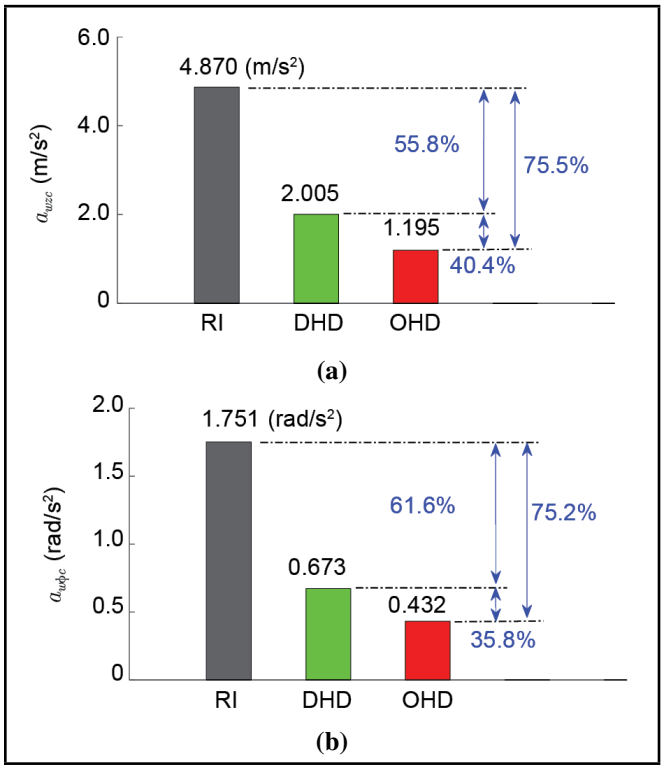

Figure 12. (a) Vertical RMS acceleration. (b) Pitching RMS acceleration of cab.

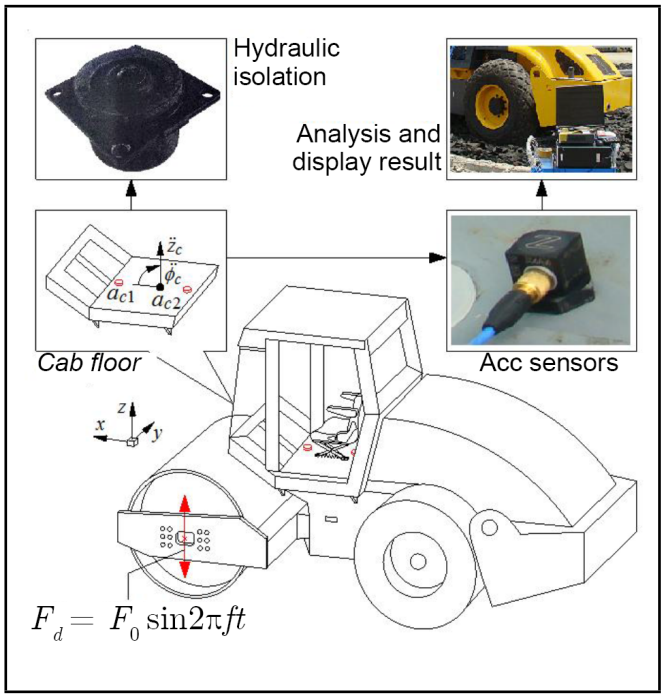

Figure 13. The measurement diagram of the vibratory roller cab.

and 77.0%.

Besides, based on the results of the PSD of the cab's vertical and pitching acceleration responses in Fig. 11, the computed and compared results of a_{wzc} and $a_{w\phi c}$ between RI, DHD, and OHD are presented in Figs. 12a and 12b.

Results in Fig. 12 also show that both a_{wzc} and $a_{w\phi c}$ with OHD are lower than those of RI and DHD. Especially, a_{wzc} and $a_{w\phi c}$ with OHD are remarkably decreased by 40.4% and 35.8% in comparison with DHD and by 75.5% and 75.2% compared to RI. These analysis results imply that with the OHD is added into the cab's rubber isolations, the cab's ride comfort and shaking are strongly improved in comparison with the cab's rubber isolations under the different excitation frequencies of the vibratory roller cab.

4.3. Experimental Study of OHD

To demonstrate the practical effectiveness of OHD added into the cab's isolations, a simple experiment of the vibratory roller with its cab isolations equipped with RI, DHD, and OHD is performed. During the test, the engine is on. However, the engine rotates at high frequency and very small vibration amplitude with its harmonic excitation. Besides, the engine's isolation system is also used by the good hydraulic mounts. Therefore, the engine's vibration has very little effect on the cab vibration. The cab's vibration was mainly affected by the excitations of the low frequency and high vibration amplitude of the vibratory drum and the elastic deformation of the random ground surface when the vibratory roller is moving and working. Therefore, the vibratory roller was measured under an harmonic excitation force of the drum ($F_d = F_0 \sin 2\pi ft$) at 28 Hz when the vibratory roller is moving and working on elastic deformation ground of rubber material at 3.0 km/h. The measurement diagram of the vibratory roller cab is plotted in Fig. 13.

To measure the vertical power-spectral-density (PSD) acceleration and pitching PSD acceleration of the cab, two three-dimensional sensors have been installed at the front cab floor and rear cab floor at the positions of the cab's isolation mounts to determine the vertical accelerations (a_{c1} and a_{c2}) of the front and rear cab floor (see Fig. 13). From the two measured accelerations of a_{c1} and a_{c2}, the vertical acceleration and pitching acceleration of the cab are calculated by:

$$\begin{cases} \ddot{z}_c = a_{c1} - l_1\ddot{\phi}_c = a_{c2} - l_2\ddot{\phi}_c \\ \ddot{\phi}_c = (a_{c1} - a_{c2})/l_c \end{cases}; \tag{15}$$

where $l_c = l_{c1} + l_{c2}$ and both l_{c1} and l_{c2} are calculated in Table 1.

The measured signals of the $\ddot{z}_c$ and $\ddot{\phi}$ are then transmitted to Belgium-LMS-dynamic-test to calculate measurement results of the vertical PSD acceleration and pitching PSD acceleration of the cab. Based on the measured and computed results with RI, DHD, and OHD, the PSD of the cab's vertical and pitching accelerations are given in Figs. 14a and 14b.

Like the simulation results between RI, DHD, and OHD in section 4.2, the experiment also shows that with RI used, the amplitude-frequency responses of the cab's vertical PSD acceleration and pitching PSD acceleration at the resonant frequencies are very high. However, with DHD and OHD added, their amplitude-frequency responses are strongly reduced in comparison with RI nder the excitation frequencies, especially with ODH. Based on the simulation and experiment results of OHD added in the cab's rubber isolations, the study shows that the cab's ride comfort and shaking are remarkably improved compared to the cab's traditional isolations using rubber materials. Therefore, OHD should be studied and applied to replace the cab's RI to improve the vibratory roller's ride quality.

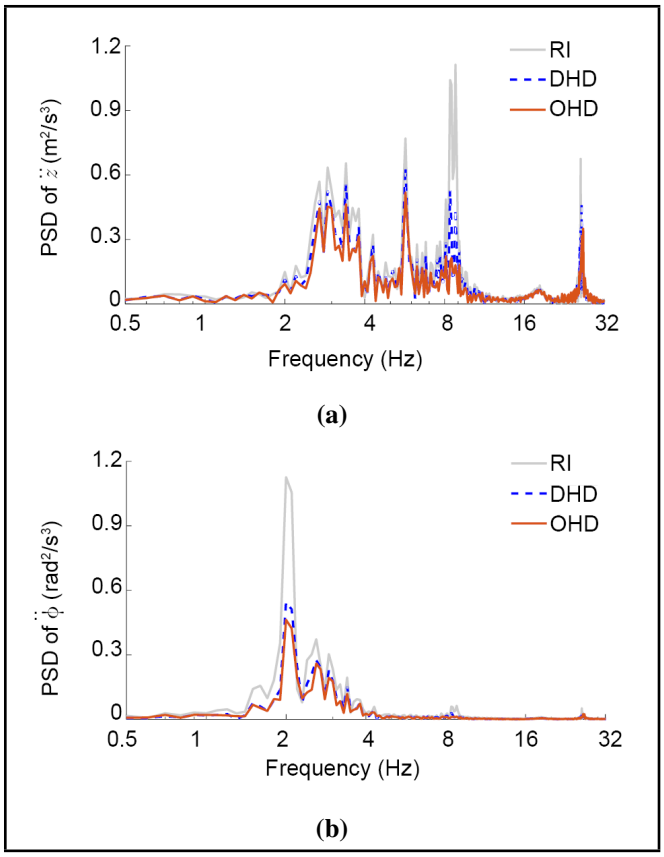

Figure 14. (a) The experimental result of the vibratory roller cab using RI, DHD, and OHD; Vertical PSD acceleration. (b) Pitching PSD acceleration of cab.

5. CONCLUSIONS

With the cab's isolation using the rubber materials, the damping values of the cab's RI are very low. Thus, to ensure the vibratory roller's ride comfort, these damping values need to be designed in the range of $21.8 \times 10^3 \leq c_{r1} \leq 43.6 \times 10^3$ and $2.9 \times 10^3 \leq c_{r2} \leq 5.8 \times 10^3$ Nsm^{-1}.

With adding the quadratic damping values of DHD into the cab's RI, both the cab's vertical vibration and sharking are greatly affected by the change of $C_h = [c_{h1}, c_{h2}]$ and damping ratio β in DHD. To improve the cab's vertical vibration and sharking, these values should be designed in the range of $6 \times 10^3 < c_{h1} < c_{h2} < 4.95 \times 10^3$ Ns^{2}m^{-2}, and $1.0 < \beta < 3.0$.

The quadratic damping values of $C_h = [c_{h1}, c_{h2}]$ depend greatly on the geometric dimensions of the chamber diameter (D_1) and annular gap (H) in the hydraulic dampers. With the dynamic parameters of D_1, H, c_{h1}, c_{h2}, and β optimized by GA, the maximum values of the PSD of the cab's vertical and pitching accelerations are strongly reduced by 94.3% and 77.0% in comparison with RI. Besides, both a_{wzc} and $a_{w\phi c}$ with OHD are also greatly decreased by 75.5% and 75.2% compared to RI. Additionally, the experiment results also show that the maximum values of the PSD of the cab's vertical and pitching accelerations with OHD are also lower than those of the cab's RI and DHD. Therefore, with OHD added into the cab's RI, the cab's ride comfort and shaking are remarkably ameliorated under the different excitation frequencies of the vibratory roller cab. From this study result, OHD should be added to the cab's rubber isolations to improve the vibratory roller's ride quality.

REFERENCES

[1] Tateyama, K. Ashida, S., Fukagawa, R. and Takahashi, H. Geomechatronics — Interaction between ground and construction machinery and its application to construction robotics, *Journal of Terramechanics*, **43**, 341–353, (2006). https://doi.org/10.1016/j.jterra.2005.05.008

[2] Le, V. Q. *Vibration study and control for cab of vibratory roller*, Southeast University, (2013).

[3] Yang, J., Wang, X., Lu, J., et al. Performance study of semi-active seat suspension added by quasi-zero stiffness structure under various vibratory roller models, *Proc. IMechE, Part D: Journal of Automobile Engineering*, **238**, 1129–1143, (2024). https://doi.org/10.1177/09544070221143167

[4] Harrison and Robin, T. Formulation of a noise standard for off-road vehicles. *The Journal of the Acoustical Society of America*, **55**, 484, (1974). https://doi.org/10.1121/1.3438038

[5] Santhosh, S. A. Velmurugan, V. A. Paramasivam, V. B. and Thanikaikarasan, S. C. Experimental investigation and comparative analysis of rubber engine mount vibration and noise characteristics, *Materials Today: Proceedings*, **21**, 638–642, (2020). https://doi.org/10.1016/j.matpr.2019.06.730

[6] Zhang, L., Nguyen, V., Wang, C., Xu, S. et al. Review eesearch on isolation systems of the cab and driver's seat in soil compactors, *SAE International Journal of Vehicle Dynamics, Stability, and NVH*, **7**, 115–136, (2023). https://doi.org/10.4271/10-07-02-0008

[7] Zheng, Y. S. Zhang, X. N. Luo, Y. J. et al., Design and experiment of a high-static–low-dynamic stiffness isolator using a negative stiffness magnetic spring, *Journal of Sound and Vibration*, **360**, 31–52, (2016). https://doi.org/10.1016/j.jsv.2015.09.019

[8] Ming, S. L., Qiang, R. J., Ni, D. K., et al. Isolation efficiency of vehicle seat suspension with three quasi-zero stiffness models, *International Journal of Acoustics and Vibration*, **27**, 210–220, (2022). https://doi.org/10.20855/ijav.2022. 27.31858

[9] Van, L. N. and Deng, K. N. Method of improving the soil compactor's ride quality based on the optimal negative stiffness structure, *International Journal of Vehicle Design*, **91**, 181–207, (2023). https://doi.org/10.1504/IJVD.2023.131052

[10] Ye, T. F., Li, S. M., et al. Enhancing the vibratory roller's ride comfort with semi-active seat suspension embedded by quasi-zero stiffness structure, *International Journal Dynamics and Control*, **11**, 2069–2081, (2023). https://doi.org/10.1007/s40435-023-01127-3

[11] Benjamin, B., Jason, T., D., and Rajendra, S. Experimental study of hydraulic engine mounts using multiple inertia tracks and orifices: Narrow and broad band tuning concepts, *Journal of Sound and Vibration*, **331**, 5209–5223, (2012). https://doi.org/10.1016/j.jsv.2012.07.001

[12] Yi, F. Y. and Xie, M. Z. Objective evaluation of engine mounting isolation, *AASRI Procedia*, **3**, 49–53, (2012). https://doi.org/10.1016/j.aasri.2012.11.009

[13] Hosseini, S. S. and Marzbanrad, J. Robust H-infinity controller in a MRF engine mount for improving the vehicle ride comfort, *International Journal of Acoustics and Vibration*, **25**, 219–225, (2020). https://doi.org/10.20855/ijav.2020. 25.21592

[14] Wang, M., Yao, G. F., Zhao, J. Z., and Qin, M. A novel design of semi-active hydraulic mount with wide-band tunable notch frequency, *Journal of Sound and Vibration*, **333**, 2196–2211, (2014). https://doi.org/10.1016/j.jsv.2013.12.004

[15] Fabian, H., Christian, S., Peter, P., et al. Experimental and analytical study of secondary path variations in active engine mounts, *Journal of Sound and Vibration*, **340**, 22–38, (2015). https://doi.org/10.1016/j.jsv.2014.11.024

[16] Guo, R., Wei, X. K., and Gao, J. Extended filtered-x-least-mean-squares algorithm for an active control engine mount based on acceleration error signal, *Advances in Mechanical Engineering*, **9**, 117287861, (2017). https://doi.org/10.1177/1687814017724350

[17] Jia, Z. B. Zheng, X. Zhou, Q., et al. A hybrid active noise control system for the attenuation of road noise inside a vehicle cabin, *Sensors*, **20**, 1–15, (2020). https://doi.org/10.3390/ s20247190

[18] Ke, N. D., Qiang, R. J., Run, Z. J., et al. Enhancing the ride comfort of off-road vibratory rollers with seat suspension using optimal quasi-zero stiffness, *Proc. IMechE, Part C: Journal of Mechanical Engineering Science*, **237**, 482–496, (2023). https://doi.org/10.1177/09544062221119929

[19] Jiao, S., Wang, Y., Zhang, L. and Hua, H. Shock wave characteristics of a hydraulic damper for shock test machine, *Mechanical Systems and Signal Processing*, **24**, 1570–1578, (2010). https://doi.org/10.1016/j.ymssp.2009. 12.005

[20] Zhang, Y., Chen, H., Guo, K., et al. Electro-hydraulic damper for energy harvesting suspension: Modeling, prototyping and experimental validation, *Applied Energy*, **199**, 1–12, (2017). https://doi.org/10.1016/j.apenergy.2017.04.085

[21] Nguyen, V. L., Zhang. J. R. and Yang. X. Z. Low-frequency performance analysis of semi-active cab's hydraulic mounts of an off-road vibratory roller, *Shock and Vibration*, **2019**, 1–15, (2019). https://doi.org/10.1155/2019/87253 82

[22] Zhao, J., Yin, Y., Chen, J., Zhao, W. et al. Evaluation and prediction of vibration comfort in engineering machinery cabs using random forest with genetic algorithm, *SAE International Journal of Vehicle Dynamics, Stability, and NVH*, **8**, 491–512, (2024). https://doi.org/10.4271/10-08-04-0027

[23] Jiang, J., Van, L., Xu, S., and Xu, X. Isolating efficiency of soil compactor's seat suspension using optimal negative stiffness structure under various deformable terrains, *SAE International Journal of Vehicle Dynamics, Stability, and NVH*, **6**, 209–221, (2022). https://doi.org/10.4271/10-06-03-0014

[24] Jiao, R. Q. and Van, L. N. Studies on the low frequency vibration of the suspension system for heavy trucks under different operation conditions, *Noise & Vibration Worldwide*, **52**, 127–136, (2020). https://doi.org/10.1177/0957456520948271

[25] Nguyen, V. L. *Study on semi-active control for cab's hydraulic isolation system of the vibratory roller*, Southeast University, (2018).

[26] ISO 8068. *Mechanical Vibration—Road Surface Profiles —Reporting of Measured Data*, Geneve, Switzerland, International Organization for Standardization, (1995).

[27] ISO 2631-1. *Mechanical vibration and shock—Evaluation of human exposure to wholebody vibration—Part* 1: General requirements. Geneve, Switzerland, International Organization for Standardization, (1997).

[28] Kat, C., Skrickij, V., Shyrokau, B., Kojis, P. et al. Vibration-induced discomfort in vehicles: A comparative evaluation approach for enhancing comfort and ride quality, *SAE International Journal of Vehicle Dynamics, Stability, and NVH*, **8**, 139–153, (2024). https://doi.org/10.4271/10-08-02-0009

[29] Aakii, G. and Ztürk, F. Kinematics & compliance validation of a vehicle suspension and steering kinematics optimization using neural networks, *Mechanika*, **29**, 243–251, (2023). https://doi.org/10.5755/j02.mech.31983

[30] Shehata Gad, A., Darakhshan Jabeen, S., and Galal Ata, W. Damping magnetorheological systems based on optimal neural networks preview control integrated with new hybrid fuzzy controller to improve ride comfort, *SAE International Journal of Vehicle Dynamics, Stability, and NVH*, **7**, 489–512, (2023). https://doi.org/10.4271/10-07-04-0032